Magnetoelectric signature in the magnetic properties of antiferromagnetic multiferroics: Atomistic simulations and phenomenology

Dovran Rahmedov,[1] Sergey Prosandeev,[1] Jorge Íñiguez,[2] and L. Bellaiche[1]

[1]*Physics Department, University of Arkansas and Institute for Nanoscience and Engineering, Fayetteville, Arkansas 72701, USA*

[2]*Institut de Ciència de Materials de Barcelona (ICMAB-CSIC), Campus UAB, 08193 Bellaterra, Spain*

(Received 2 October 2013; published 4 December 2013)

An effective Hamiltonian approach is used to reveal the effects of the (biquadratic) magnetoelectric (ME) coupling between local electric dipoles and local magnetic moments on magnetic properties of antiferromagnetic multiferroics. In addition to showing that the Néel magnetic ordering temperature (T_N) can strongly depend on such coupling, the simulations also reveal that the perpendicular component of the magnetic susceptibility, $\chi_{M,\perp}$, can present some strong deviations from that of a typical antiferromagnet because of the ME coupling. Examples of systems for which T_N is lower than the first-order paraelectric-to-ferroelectric transition temperature (T_C) are (1) a discontinuity of $\chi_{M,\perp}$ at T_C; (2) the inverse of the magnetic susceptibility not following anymore the traditional Curie law when the temperature ranges between T_N and T_C; and (3) $\chi_{M,\perp}$ increasing with temperature, rather than forming a plateau, when the system is heated up to T_N. A Landau-type phenomenological model is further developed to reproduce and understand all these effects.

DOI: 10.1103/PhysRevB.88.224405 PACS number(s): 75.85.+t, 75.50.Ee, 75.10.−b

I. INTRODUCTION

Antiferromagnetic (AFM) compounds are numerous in nature, and form an important class of materials[1] that can find application in some technologies. Examples include spin-valve devices that take advantage of the so-called exchange bias.[2,3] AFM systems can also exhibit interesting "universal" phenomena such as the perpendicular component of the magnetic susceptibility, $\chi_{M,\perp}$, (1) being inversely proportional to $T + T_N$ for temperature T above the T_N Néel ordering temperature, and (2) adopting a kind of plateau for temperature smaller than T_N.[4,5] Note that the wordings "perpendicular component" refer to a component that is associated with a direction being perpendicular to the AFM vector.

Interestingly, many multiferroic materials, that can simultaneously exhibit electric polarization and magnetic ordering, are antiferromagnetic. Multiferroics were investigated from the 1960s to the 1980s[6–10] and have attracted renewed attention since around 10 years ago (see, e.g., Refs. 11–25), because of the inherent magnetoelectric (ME) coupling between magnetic and electric dipoles. The effect of these ME couplings on electrical or structural-related properties have been reported in some previous works, including the kink in the dielectric constant at around the magnetic ordering temperature[20,26] or phonon anomalies observed around T_N.[18] On the other hand, we are not aware that the effects of ME coupling on *magnetic* properties have been revealed and understood. For instance, one may wonder whether the Néel temperature is sensitive to the strength of the ME coupling, and whether the aforementioned universal features (1) and (2) of $\chi_{M,\perp}$ still hold in an AFM multiferroics.

The goal of this paper is to address such issues, by performing numerical simulations on a model antiferromagnetic multiferroic and by allowing the strength of the ME couplings to vary in this system. As we are going to see, surprises are in store. Moreover, these surprises can be easily explained by a rather simple phenomenological model that is further developed to analyze the numerical data.

This paper is organized as follows. Section II gives details about the numerical method that is used here. Section III shows the results arising from the use of this method, as well as provides the development of a Landau-type phenomenology that allows us to deeply understand such results. Finally, a summary is given in Sec. IV.

II. NUMERICAL METHOD

Our "numerical toy model" originates from the effective Hamiltonian of $BiFeO_3$ (BFO) developed in Refs. 20,21. More precisely, the total energy, E_{tot}, is written as

$$E_{\text{tot}} = E_{\text{struct}}(\{\mathbf{u}_i\},\{\eta_i\},\{\omega_i\}) + E_{\text{Mag}}(\{\mathbf{m}_i\},\{\mathbf{u}_i\}), \quad (1)$$

where the first term, E_{struct}, gathers energies associated with structural degrees of freedom and their mutual interactions. These structural degrees of freedom are (i) the $\mathbf{u}_i$ local soft mode in unit cell i, which is directly proportional to the electrical dipole centered on that site; (ii) the η_i strain in unit cell i, that contains homogeneous and inhomogeneous parts;[27] and (iii) the $\{\omega_i\}$ vector that characterizes the oxygen octahedral tilting in unit cell i. The analytic form of E_{struct} is given in Ref. 28. The second term of Eq. (1), E_{Mag}, gathers the interactions between the $\mathbf{m}_i$ magnetic moments of Fe ions at different cells i, and the interactions between these magnetic moments and the local soft modes. The analytical expression of E_{Mag} is the one provided in Ref. 21 with the exception that the interactions between magnetic moments and both the strains and oxygen octahedral tiltings are neglected here (which slightly simplifies our atomistic tool with respect to the real effective Hamiltonian of BFO, in order to determine the sole effects of ME couplings on physical properties). E_{Mag} thus reads

$$E_{\text{Mag}}(\{\mathbf{m}_i\},\{\mathbf{u}_i\}) = \sum_{i,j,\alpha,\gamma} D_{ij,\alpha\gamma} m_{i,\alpha} m_{j,\gamma} + \sum_{i,j,\alpha,\gamma,\nu,\delta} E_{ij,\alpha\gamma\nu\delta} m_{i,\alpha} m_{j,\gamma} u_{i,\nu} u_{i,\delta}, \quad (2)$$

where α, γ, ν, and δ denote Cartesian components. The sums over i run over all the Fe sites while the sums over j run over the first, second, and third nearest neighbors of the Fe site i. The first term of $E_{\rm Mag}$ represents the exchange interactions between magnetic moments at sites i and j. The second term represents how the local soft mode affects these magnetic exchange interactions, which is precisely the (biquadratic) ME coupling that we are going to study here. This latter coupling is allowed by symmetry in *any* multiferroic material, which implies that our results should be of general nature. Note, however, that the predictions of this paper are technically valid for the (numerous) multiferroics for which the paraelectric-to-ferroelectric transition temperature is higher than the magnetic Néel temperature. This is because our toy model originates from the effective Hamiltonian of BFO, which is a material for which such hierarchy in temperature exists. A brief discussion is provided at the end of this paper to address other cases.

All the parameters entering the analytical expression of $E_{\rm tot}$ (including the D_{ij} coefficients) are extracted from first-principles calculations on $BiFeO_3$,[29] with the sole exception of the E_{ij} parameters that are allowed to vary from their first-principles values—in order to precisely assert the effect of the ME coupling on electric and magnetic properties.

Monte Carlo (MC) simulations using $E_{\rm tot}$ for the internal energy are performed on a $14 \times 14 \times 14$ supercell, with the local magnetic moments $\{\mathbf{m}_i\}$ having a fixed magnitude of $4\mu_B$ (as consistent with first-principles computations of BFO[13]). Practically, the system is cooled down to very low temperature (of the order of a Kelvin) under an electric field that is applied along the pseudocubic [111] direction, in order to reach an $R3c$ ground state. Then, this field is removed and the temperature is increased until reaching 1300 K. The numerical results shown here correspond to this increase-in-temperature path under no field.

III. RESULTS

A. Atomistic simulations

In the present study, three different physical quantities are determined: (1) the G-type antiferromagnetic vector, which is defined as $\mathbf{L} = \frac{1}{N}\sum_i \mathbf{m}_i(-1)^{n_x(i)+n_y(i)+n_z(i)}$, where the sum runs over all the Fe sites and where $n_x(i)$, $n_y(i)$, and $n_z(i)$ are integers locating the cell i (more precisely, the Fe site i is centered at $[n_x(i)\mathbf{x} + n_y(i)\mathbf{y} + n_z(i)\mathbf{z}]a$, where a is the 5-atom lattice constant and where $\mathbf{x}$, $\mathbf{y}$, and $\mathbf{z}$ are unit vectors along the Cartesian axes); (2) the $\mathbf{u}$ supercell average of the $\{\mathbf{u}_i\}$ local soft modes, which is directly proportional to the spontaneous polarization; and (3) the perpendicular component of the magnetic susceptibility, $\chi_{M,\perp}$, which is computed as the linear slope of the function representing the dependence of the magnetization (which is simply the supercell average of the $\{\mathbf{m}_i\}$'s) on an applied magnetic field. This latter field is oriented along the [111] pseudocubic direction, that is along the polarization direction while being perpendicular to the G-type AFM vector of BFO.[21] The applied magnetic field is allowed to have a magnitude ranging between zero and 100 T, in order to precisely compute $\chi_{M,\perp}$. Figures 1, 2, and 3 show the magnitude of $\mathbf{L}$, the magnitude of $\mathbf{u}$, and $\chi_{M,\perp}$, respectively,

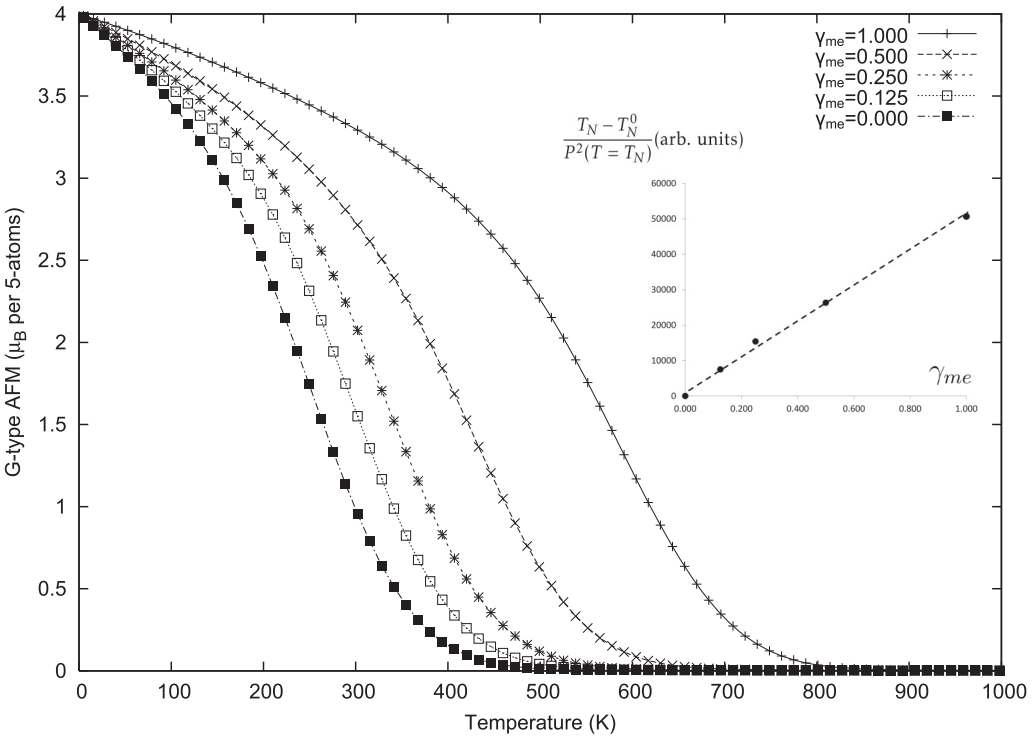

FIG. 1. Temperature dependency of the magnitude of the G-type antiferromagnetic vector, for five different selected sets of the ME-related E_{ij} parameters of Eq. (2). The numerical data are shown by symbols while the lines are guides for the eye. The inset shows $\frac{T_N - T_N^0}{P^2(T=T_N)}$ as a function of γ_{me}, where $P^2(T = T_N)$ is the square of the polarization at the Néel temperature and where T_N^0 is the "bare" Néel temperature (i.e., in the case of no ME coupling, that is corresponding to $\gamma_{me} = 0$). This inset confirms the validity of the phenomenological equation (9).

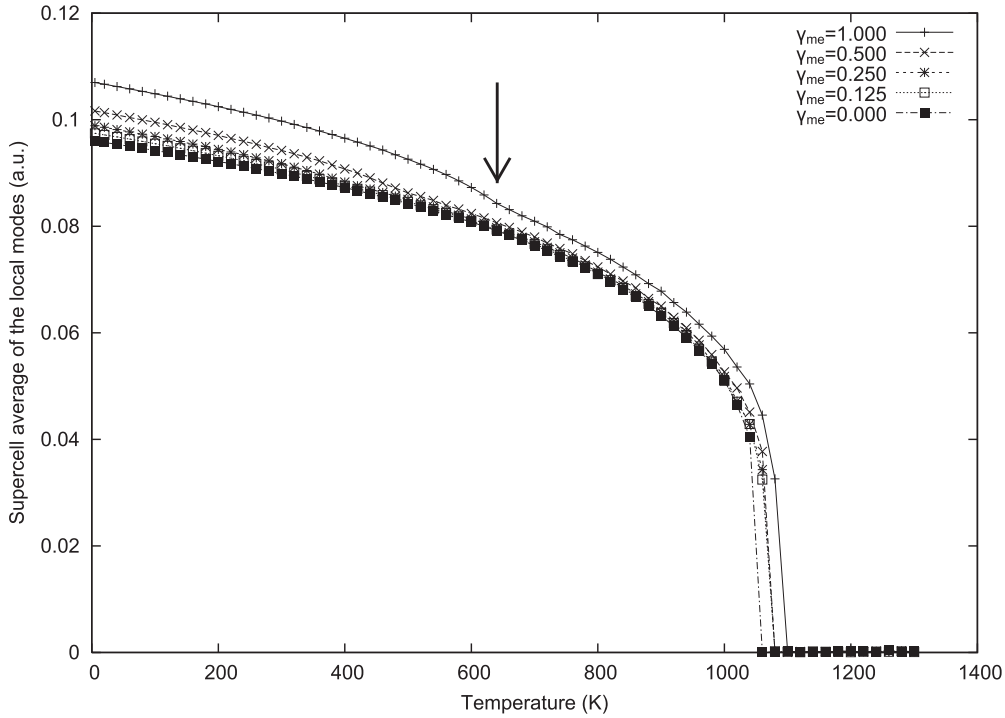

FIG. 2. Same as Fig. 1, but for the magnitude of the supercell average of the local modes. The arrow shows the location of the Néel temperature when $E_{ij} = E_{ij,\mathrm{ref}}$ (or, equivalently, $\gamma_{me} = 1$).

as a function of temperature for five different sets of E_{ij} coefficients. If we denote the first-principles values of the E_{ij} coefficients in BFO as $E_{ij,\mathrm{ref}}$, then these five sets correspond to E_{ij} being equal to $\gamma_{me} E_{ij,\mathrm{ref}}$, with $\gamma_{me} = 1, 0.5, 0.25, 0.125$, and 0.0, respectively (as characteristic of progressively weaker magnetoelectric couplings until they fully vanish).

Figure 1 reveals that the Néel temperature, T_N (which is taken as the temperature at which the magnitude of $\mathbf{L}$ possesses an inflection point) strongly increases when the magnetoelectric coefficients grow in strength: for $\gamma_{me} = 0$, it is about 275 K (this temperature will be denoted as T_N^0 in the following) while it significantly increases up to 635 K when $\gamma_{me} = 1$. Another effect that is visible in Fig. 1 is the enhancement of the AFM vector resulting from the increase of γ_{me} for any temperature below $T_N^0 = 275$ K (with the sole exception of 0 K for which the antiferromagnetic vectors are all equal to $4\mu_B$ in magnitude, as consistent with quantum mechanics).

Furthermore, Fig. 2 shows that the Curie temperature, T_C, which is the temperature at which the polarization suddenly jumps from a vanishing to nonzero value (via a first-order transition), is less sensitive to the ME couplings: T_C varies from 1050 K to 1090 K when the γ_{me} coefficient changes from 0 to 1. However, Fig. 2 also demonstrates that the polarization-versus-temperature dependence changes its curvature around T_N. This effect is more pronounced for stronger γ_{me}, therefore indicating a significant effect of ME couplings on some *electric* properties.

In addition to Fig. 1, another consequence of ME couplings on magnetic properties can be clearly seen from Fig. 3. As a matter of fact, in the case of $\gamma_{me} = 0$, the magnetic susceptibility adopts the "normal" behavior inherent to antiferromagnetic systems,[4] that is a kind of a plateau for temperatures lower than T_N^0 and then a monotonic decrease (that we numerically found to be inversely proportional to $T + T_N^0$, as consistent with Refs. 4,5) when heating the systems above T_N^0. In contrast, switching on the ME couplings has three dramatic effects: (1) the value of the magnetic susceptibility decreases as the ME couplings increase in strength for any temperature $T \leqslant T_N^0$, with the plateau occurring when $\gamma_{me} = 0$, being even replaced by a slightly increasing function when increasing the temperature up to T_N^0 for the largest studied γ_{me} parameters; (2) the magnetic susceptibility is not anymore inversely proportional to $T + T_N$ when heating the system from T_N to T_C. In fact, $\chi_{M,\perp}$ is found to be nearly independent of temperature for the strongest γ_{me} coefficients; and (3) a sudden jump of $\chi_{M,\perp}$ is clearly seen at the Curie temperature.

B. Phenomenology

To reveal the origins of all these effects and better understand them, let us develop a phenomenology for which the free energy, $\mathcal{F}$, is given by

$$\mathcal{F} = \mathcal{F}_0 + \frac{A_2}{2}P^2 + \frac{A_4}{4}P^4 + \frac{A_6}{6}P^6 + \frac{B_2}{2}M^2 + \frac{C_2}{2}L^2 + \frac{C_4}{4}L^4 + \frac{\beta_{PM}}{2}P^2M^2 + \frac{\beta_{PL}}{2}P^2L^2 + \frac{\beta_{LM}}{2}L^2M^2 - MH, \quad (3)$$

where M and L are the magnetization and G-type antiferromagnetic moment, respectively, while P and H are the electrical polarization and applied magnetic field, respectively. Note that, in the case of the simulations described above, the polarization, induced magnetization, and magnetic field are all along the pseudocubic [111] direction while the AFM vector is

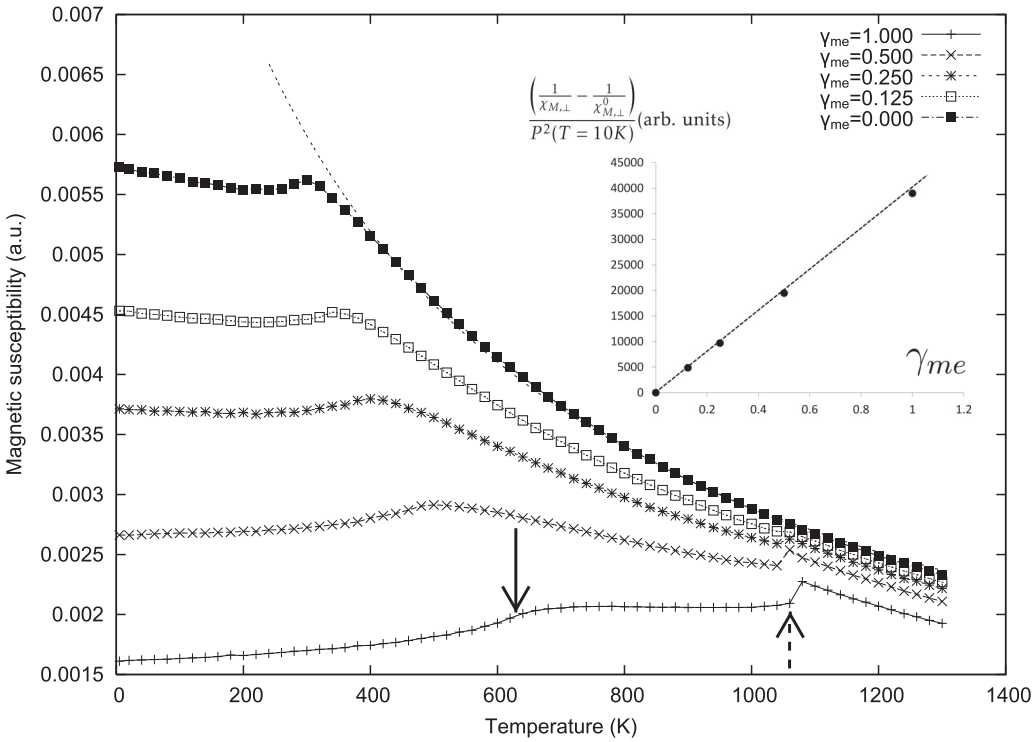

FIG. 3. Same as Figs. 1 and 2, but for the perpendicular component of the magnetic susceptibility. The dashed line shows the fit of the magnetic susceptibility by $\frac{b_2}{T+T_N^0}$, in the case of *no* ME coupling. The solid and dashed arrows depict the values of T_N and T_C, respectively, when $E_{ij} = E_{ij,\mathrm{ref}}$ (or, equivalently, $\gamma_{me} = 1$). The inset displays $(\frac{1}{\chi_{M,\perp}} - \frac{1}{\chi^0_{M,\perp}})/P^2(T = 10\ \mathrm{K})$ as a function of γ_{me} (see text), where $P^2(T = 10\ \mathrm{K})$ is the square of the polarization at 10 K. This inset demonstrates that the phenomenological equation (15) is obeyed.

along a direction being perpendicular to [111]. As a result, we are only concerned about the magnitude, rather than direction, of the physical quantities appearing in Eq. (3). Note that previous phenomenologies have already been developed for multiferroics; see, e.g., Refs. 30–33. As in Ref. 33 but unlike in Refs. 30–32, Eq. (3) incorporates the couplings between the polarization with *both* the magnetization and antiferromagnetic vector. This is because we are, e.g., interested in revealing the effect of ME couplings on the magnetic susceptibility of antiferromagnetic multiferroics.

As consistent with phenomenologies of antiferromagnets undergoing a second-order magnetic transition and of ferroelectrics undergoing a first-order structural transition, the C_4 and A_6 coefficients are both positive and constant, while the A_4 parameter is also constant but is negative.[5] On the other hand, the C_2, B_2, and A_2 coefficients are *temperature dependent*:[5]

$$\begin{aligned} C_2 &= c_2\big(T - T_N^0\big), \\ B_2 &= b_2\big(T + T_N^0\big), \\ A_2 &= a_2\big(T - T_C^0\big), \end{aligned} \tag{4}$$

where c_2, b_2, and a_2 are positive constants, and with T_C^0 being related to the "bare" Curie temperature, i.e., corresponding to the case of *no* ME coupling.[34] Notice the difference in sign in front of T_N^0 between the first and second line of Eq. (4).

Moreover, the β_{PL} coefficient of Eq. (3) is considered here to be a *negative* constant, since Figs. 1 and 2 show that increasing γ_{me} results in an enhancement of both L and P (at a fixed temperature below T_N^0). This enhancement also implies that the electric-dipole-mediated exchange parameters appearing in the second energy term of Eq. (2) disfavor ferromagnetism even more when γ_{me} increases in magnitude. As a result, the β_{PM} coefficient is positive, and enhancing the strength of the E_{ij} coefficients of Eq. (2) (or equivalently, γ_{me}) increases the magnitude of both the β_{PL} and β_{PM} parameters of Eq. (3). Finally, the β_{LM} parameter is a *positive* constant, as characteristic of a competition between the magnetization and AFM vector.

If we take into account that, *for temperatures below* T_C, $A_6(\beta_{PL}L^2 + A_2)$ is negative and that the magnetization always vanishes in the studied AFM system under no field, the minimization of Eq. (3) with respect to P gives

$$P^2 = \frac{-A_4 + \sqrt{A_4^2 - 4A_6(\beta_{PL}L^2 + A_2)}}{2A_6} \quad \text{for} \quad T \leqslant T_C. \tag{5}$$

Inserting Eq. (4) into Eq. (5), and distinguishing the temperature ranges below and above the Néel temperature (at which the AFM vector vanishes), thus gives

$$\begin{aligned} P^2 &= \frac{-A_4 + \sqrt{A_4^2 + 4A_6a_2\big(T_C^0 - T\big)}}{2A_6} \quad \text{for } T_N \leqslant T \leqslant T_C, \\ P^2 &= \frac{-A_4 + \sqrt{A_4^2 + 4A_6a_2\big(T_C^0 - T\big) - 4A_6\beta_{PL}L^2}}{2A_6} \\ &\text{for } T \leqslant T_N \leqslant T_C. \end{aligned} \tag{6}$$

The fact that the first and second lines of Eq. (6) differ by the presence of $-4A_6\beta_{PL}L^2$ under the square root (which is a quantity that is always positive) successfully explains the upward change of slope in the polarization-versus-temperature curves of Fig. 2 below T_N, when the ME effect is turned on (that is when the β_{PL} coefficient does not vanish), since L is also temperature dependent—as shown in Fig. 1. Our Landau-type phenomenological model can therefore reproduce and explain some striking features revealed by the atomistic simulations.

Furthermore, minimizing Eq. (3) with respect to L in our AFM multiferroic (for which M is zero for any temperature, when no field is applied) gives

$$L^2 = \frac{-(C_2 + \beta_{PL}P^2)}{C_4} \quad \text{for} \quad T \leqslant T_N \leqslant T_C. \tag{7}$$

Inserting Eq. (4) into this latter equality then yields

$$L^2 = \frac{c_2\left(T_N^0 - T\right)}{C_4} - \frac{(\beta_{PL}P^2)}{C_4} \quad \text{for} \quad T \leqslant T_N \leqslant T_C. \tag{8}$$

Since β_{PL} is negative while C_4 is positive, the second term on the right-hand side of Eq. (8) explains another significant result of the atomistic simulations, namely why increasing γ_{me} enhances the magnitude of the AFM vector L for any finite temperature below T_N (see Fig. 1). Moreover, setting Eq. (8) to zero provides the "renormalized" Néel temperature, that is the Néel temperature that takes into account ME effects:

$$T_N = T_N^0 - \frac{(\beta_{PL}P^2)}{c_2}. \tag{9}$$

This equation indicates that the difference between T_N and T_N^0 should be proportional to both γ_{me} and the square of the polarization (computed at the Néel temperature). As shown in the inset of Fig. 1, such proportionality is well satisfied by the results of the atomistic simulations. Equation (9), which is derived from a Landau-type-model, thus provides a successful explanation of some key features of Fig. 1 (that arise from atomistic calculations), namely (1) why the Néel temperature is larger than the "bare" Néel temperature, T_N^0, when ME effects are switched on; and (2) why T_N increases when increasing γ_{me}. It would therefore be a mistake to determine the bare magnetic exchange parameters from the experimental Néel temperature of multiferroics, especially if these latter exhibit strong ME parameters.

Let us now try to explain and deeply understand some striking results shown in Fig. 3. For that, one first has to minimize Eq. (3) with respect to M:

$$M = \frac{H}{B_2 + \beta_{LM}L^2 + \beta_{PM}P^2}. \tag{10}$$

Taking the derivative of this latter equality with respect to H then gives

$$\chi_{M,\perp} = \frac{1}{B_2 + \beta_{LM}L^2 + \beta_{PM}P^2}. \tag{11}$$

This latter equation can be separated into three different equalities, depending on the range of temperatures for which the AFM vector and/or polarization vanish or not:

$$\begin{aligned}
\chi_{M,\perp} &= \frac{1}{B_2} \quad \text{for} \quad T_N \leqslant T_C \leqslant T, \\
\chi_{M,\perp} &= \frac{1}{B_2 + \beta_{PM}P^2} \quad \text{for} \quad T_N \leqslant T \leqslant T_C, \\
\chi_{M,\perp} &= \frac{1}{B_2 + \beta_{LM}L^2 + \beta_{PM}P^2} \quad \text{for} \quad T \leqslant T_N \leqslant T_C.
\end{aligned} \tag{12}$$

The first and second lines of Eq. (12) indicate that the inverse of the magnetic susceptibility should exhibit a sudden change of $\beta_{PM}P^2$ at the ferroelectric phase transition, when the polarization appears via a first-order transition. Such feature therefore explains the significant increase of χ_M numerically found when increasing the temperature through the Curie temperature, for the largest studied ME coefficients (see Fig. 3).[37]

Moreover, inserting the second line of Eq. (4) and the first line of Eq. (6) into the second line of Eq. (12) gives

$$\chi_{M,\perp} = \frac{1}{b_2\left(T + T_N^0\right) + \beta_{PM}\left\{\frac{-A_4 + \sqrt{A_4^2 + 4A_6a_2(T_C^0 - T)}}{2A_6}\right\}} \quad \text{for} \quad T_N \leqslant T \leqslant T_C. \tag{13}$$

This latter equation indicates that the magnetic susceptibility follows the "usual" $\frac{1}{b_2(T+T_N^0)}$ behavior when there is no ME coupling. On the other hand, switching the β_{PM} coefficient (by making γ_{me} non-null) leads to a violation of such traditional law, and can result in unusual behavior. For instance, let us assume, for simplicity, that $4A_6a_2(T_C^0 - T)$ is much smaller than A_4^2. Then using a Taylor expansion of the square root results in the rewriting of Eq. (13) as

$$\chi_{M,\perp} = \frac{1}{\left(b_2 + \frac{\beta_{PM}a_2}{A_4}\right)T + \left(b_2T_N^0 - \frac{\beta_{PM}A_4}{A_6} - \frac{\beta_{PM}a_2T_C^0}{A_4}\right)} \quad \text{for} \quad T_N \leqslant T \leqslant T_C. \tag{14}$$

In that case, an exact cancellation of b_2 and $\frac{\beta_{PM}a_2}{A_4}$ (recall that b_2 is positive while $\frac{\beta_{PM}a_2}{A_4}$ is negative) would render the magnetic susceptibility independent of the temperature when this latter ranges between T_N and T_C, which is nearly the case for the largest investigated γ_{me} as shown by the numerical data of Fig. 3.

Finally, the insertions of Eq. (8) and of the second line of Eq. (4) into the third line of Eq. (12) result in

$$\chi_{M,\perp} = \frac{1}{\left(b_2 - \frac{\beta_{LM}c_2}{C_4}\right)T + \left(b_2 + \frac{\beta_{LM}c_2}{C_4}\right)T_N^0 + \left(\beta_{PM} - \beta_{LM}\frac{\beta_{PL}}{C_4}\right)P^2} \quad \text{for} \quad T \leqslant T_N \leqslant T_C. \tag{15}$$

If we assume that $b_2 = \frac{\beta_{LM} c_2}{C_4}$ then the magnetic susceptibility becomes independent of temperature for $T \leqslant T_N$ *when there is no ME coupling* (i.e., when $\beta_{PL} = \beta_{PM} = 0$), as nearly consistent with Fig. 3. Moreover, the last term of the denominator of Eq. (15) is positive (since β_{PL} is negative while β_{PM}, β_{LM}, and C_4 are all positive) and involves the square of the polarization. Since this latter decreases when increasing the temperature up to the Néel temperature (see Fig. 2), the phenomenological equation (15) naturally explains another numerical result, namely why $\chi_{M,\perp}$ does not exhibit anymore a plateau and, in fact, increases when heating the system to T_N for the largest considered γ_{me} coefficient.

Note that Eq. (15) also tells us that $\frac{1}{\chi_{M,\perp}} - \frac{1}{\chi^0_{M,\perp}}$, with $\chi^0_{M,\perp}$ being the magnetic susceptibility in case of *no* ME coupling, is equal to $(\beta_{PM} - \beta_{LM}\frac{\beta_{PL}}{C_4})P^2$ and thus should be directly proportional to both the γ_{me} parameter and the square of the polarization. The inset of Fig. 3 reveals that such proportionality indeed holds for the results of the atomistic simulations, which further asserts the validity of the phenomenological model developed here.

IV. CONCLUSIONS

In summary, we have demonstrated, via the use of an atomistic scheme, that magnetic properties can be strongly affected by the ME coupling in an antiferromagnet multiferroic. This includes several strong deviations of the perpendicular component of the magnetic susceptibility from the universal behavior seen in "pure" antiferromagnets. Let us also emphasize that our phenomenological model (that allowed us to reproduce and understand key features of magnetic properties of our model AFM multiferroic) can be easily extended to AFM multiferroics for which the Néel temperature is larger than the ferroelectric Curie temperature, as well as to system exhibiting a second-order paraelectric-to-ferroelectric phase transition or even to ferromagnet ferroelectrics (unlike the case we studied here). In all these situations, $\chi_{M,\perp}$ will likely exhibit anomalous features that should be reproduced and understood by these phenomenologies. We thus hope that the present work is of broad interest and deepens our current knowledge of multiferroics and antiferromagnets.

ACKNOWLEDGMENTS

This work is financially supported by NSF Grant No. DMR-1066158 for the simulations (D.R.) and ONR Grants No. N00014-11-1-0384 and No. N00014-12-1-1034 for the phenomenology (S.P). J.I. acknowledges funding from MINECO-Spain (Grants No. MAT2010-18113 and No. CSD2007-00041). Some computations were also made possible thanks to MRI Grant No. 0722625, MRI-R2 No. 0959124, and No. 0918970 from NSF.

[1] A. B. Lidiard, Rep. Prog. Phys. **17**, 201 (1954).
[2] A. E. Berkowitz and K. Takano, J. Magn. Magn. Mater. **200**, 552 (1999).
[3] W. H. Meiklejohn, J. Appl. Phys. **33**, 1328 (1962).
[4] B. D. Cullity and C. D. Graham, *Introduction to Magnetic Materials*, 2nd ed. (John Wiley & Sons, Inc., Piscataway, New Jersey, 2009).
[5] L. D. Landau and E. M. Lifshitz, *Electrodynamics of Continuous Media*, 2nd ed., Vol. 8 (Butterworth-Heinemann, Waltham, Massachusetts, US, 1984).
[6] G. A. Smolenskii and I. E. Chupis, Sov. Phys. Usp. **25**, 475 (1982).
[7] P. Fischer, M. Polomska, I. Sosnowska, and M. Szymanski, J. Phys. C **13**, 1931 (1980).
[8] S. V. Kiselev *et al.*, Sov. Phys. Dokl. **7**, 742 (1963); G. A. Smolenskii *et al.*, Sov. Phys. Solid State **2**, 2651 (1961).
[9] J. R. Teague, R. Gerson, and W. J. James, Solid State Commun. **8**, 1073 (1970).
[10] C. Tabares-Munoz, J.-P. Rivera, A. Bezinges, A. Monnier, and H. Schmid, Jpn. J. Appl. Phys. **24**, 1051 (1985).
[11] M. Fiebig, J. Phys. D: Appl. Phys. **38**, R123 (2005).
[12] A. P. Pyatakov and A. K. Zvezdin, Phys. Usp. **55**, 557 (2012).
[13] J. B. Neaton, C. Ederer, U. V. Waghmare, N. A. Spaldin, and K. M. Rabe, Phys. Rev. B **71**, 014113 (2005).
[14] T. Zhao *et al.*, Nat. Mater. **5**, 823 (2006).
[15] D. Lebeugle, D. Colson, A. Forget, M. Viret, A. M. Bataille, and A. Gukasov, Phys. Rev. Lett. **100**, 227602 (2008).
[16] S. Lee, T. Choi, W. Ratcliff, II, R. Erwin, S-W. Cheong, and V. Kiryukhin, Phys. Rev. B **78**, 100101(R) (2008).
[17] H. Bea *et al.*, Appl. Phys. Lett. **87**, 072508 (2005); Philos. Mag. Lett. **87**, 165 (2007).
[18] R. Haumont, J. Kreisel, P. Bouvier, and F. Hippert, Phys. Rev. B **73**, 132101 (2006).
[19] C. Ederer and N. A. Spaldin, Phys. Rev. B **71**, 060401 (2005).
[20] I. A. Kornev, S. Lisenkov, R. Haumont, B. Dkhil, and L. Bellaiche, Phys. Rev. Lett. **99**, 227602 (2007).
[21] D. Albrecht, S. Lisenkov, Wei Ren, D. Rahmedov, Igor A. Kornev, and L. Bellaiche, Phys. Rev. B **81**, 140401(R) (2010).
[22] J. Wang *et al.*, Science **299**, 1719 (2003).
[23] J. C. Wojdel and J. Iniguez, Phys. Rev. Lett. **103**, 267205 (2009).
[24] W. Eerenstein, N. D. Mathur, and J. F. Scott, Nature (London) **442**, 759 (2006).
[25] N. A. Spaldin and M. Fiebig, Science **309**, 391 (2005).
[26] C. Zhong, J. Fang, and Q. Jiang, J. Phys.: Condens. Matter. **16**, 9059 (2004).
[27] W. Zhong, D. Vanderbilt, and K. M. Rabe, Phys. Rev. Lett. **73**, 1861 (1994); Phys. Rev. B **52**, 6301 (1995).
[28] I. A. Kornev, L. Bellaiche, P.-E. Janolin, B. Dkhil, and E. Suard, Phys. Rev. Lett. **97**, 157601 (2006).
[29] V. I. Anisimov, F. Aryasetiawan, and A. I. Lichtenstein, J. Phys: Condens. Matter **9**, 767 (1997).
[30] M. D. Glinchuk, E. A. Eliseev, A. N. Morozovska, and R. Blinc, Phys. Rev. B **77**, 024106 (2008).
[31] G. Nénert, J. Phys.: Condens. Matter **20**, 335229 (2008).
[32] G. Nénert, U. Adem, E. M. Bauer, C. Bellitto, G. Righini, and T. T. M. Palstra, Phys. Rev. B **78**, 054443 (2008).
[33] A. A. Nugroho, N. Bellido, U. Adem, G. Nénert, Ch. Simon, M. O. Tjia, M. Mostovoy, and T. T. M. Palstra, Phys. Rev. B **75**, 174435 (2007).

[34] T_C^0 is not exactly the bare Curie temperature because the paraelectric-to-ferroelectric transition is of first order. In that case, the bare Curie temperature is equal to $T_C^0 + \frac{3A_4^2}{16a_2A_6}$ (Ref. 35). Note also that the paraelectric-to-ferroelectric transition predicted by the presently used effective Hamiltonian of BFO is rather special; namely it is a trigger-type transition that is driven by the collaborative coupling between the polarization and the tilting of oxygen octahedra (Ref. 36). As a result, the free energy is likely more complicated than the one provided in Eq. (3). However, we decided to use this latter for the sake of simplicity and because it can easily reproduce and explain several ferroelectric and magnetic anomalies for temperatures below the Curie temperature.

[35] See, e.g., http://yclept.ucdavis.edu/course/240C/Notes/Landau/LandauPhaseTrans.pdf.

[36] I. A. Kornev and L. Bellaiche, Phys. Rev. B **79**, 100105(R) (2009).

[37] Note that plugging the second line of Eq. (4) into the first line of Eq. (12) results in a magnetic susceptibility that is given by $\frac{1}{b_2(T+T_N^0)}$ for temperature above T_C. This implies that such magnetic susceptibility should be independent of the ME coupling. Figure 3 indicates that this independency is not really obeyed, therefore pointing to an inadequacy of the phenomenology introduced here for temperature at or above the Curie point. This inadequacy is further emphasized when realizing that the phenomenology also predicts that the Curie point should be insensitive to the γ_{me} parameter according to the first line of Eq. (6), which is not exactly the case (see Fig. 2). We numerically found that these deviations from the numerical data are in fact caused by *local* effects; namely, the local electric dipoles still interact with the local magnetic moments even at or above the bare Curie temperature.